

The direction of core solidification in asteroids: implications for dynamo generation.

K. H. Dodds^{1}, J. F. J. Bryson², J. A. Neufeld^{1,3,4} & R. J. Harrison¹*

¹Department of Earth Sciences, University of Cambridge, Downing Street, Cambridge, CB2 3EQ, UK. ²Department of Earth Sciences, University of Oxford, South Parks Road, Oxford, OX1 3AN, UK. ³Department of Applied Mathematics and Theoretical Physics, University of Cambridge, Centre for Mathematical Sciences, Wilberforce Road, Cambridge, CB3 0WA, UK. ⁴Institute for Energy and Environmental Flows, University of Cambridge, Madingley Road, Cambridge, CB3 0EZ, UK.

**Corresponding author. E-mail: kathryn.dodds@ens-lyon.fr Present address: LGL-TPE, École Normale Supérieure de Lyon, 46 Allée d'Italie, Lyon, 69007, France.*

This manuscript has been submitted for publication in *Icarus*. Please note that subsequent versions of this manuscript may have slightly different content. If accepted, the final version of this manuscript will be available via the '*Peer-reviewed Publication DOI*' link on the right-hand side of this webpage. Feel free to contact any of the authors as we welcome feedback.

Highlights

The direction of core solidification in asteroids: implications for dynamo generation.

K. H. Dodds, J. F. J. Bryson, J. A. Neufeld, R. J. Harrison

- The direction of core solidification controls the possible dynamo driving mechanisms.
- However, the direction of solidification in asteroid cores is currently uncertain.
- We predict that asteroid cores solidified inwardly from the core-mantle boundary.
- Due to their low pressures, a new mechanism is needed to drive last-stage asteroid core dynamos.

The direction of core solidification in asteroids: implications for dynamo generation.

K. H. Dodds^{a,*}, J. F. J. Bryson^b, J. A. Neufeld^{a,c,d}, R. J. Harrison^a

^a*Department of Earth Sciences, University of Cambridge, Downing Street, Cambridge, CB2 3EQ, U.K.*

^b*Department of Earth Sciences, University of Oxford, South Parks Road, Oxford, OX1 3AN, U.K.*

^c*Department of Applied Mathematics and Theoretical Physics, University of Cambridge, Centre for Mathematical Sciences, Wilberforce Road, Cambridge, CB3 0WA, U.K.*

^d*Institute for Energy and Environmental Flows, University of Cambridge, Madingley Road, Cambridge, CB3 0EZ, U.K.*

Abstract

Paleomagnetic studies of meteorites over the past two decades have revealed that the cores of multiple meteorite parent bodies, including those of certain chondritic groups, generated dynamo fields as they crystallised. However, uncertainties in the direction and mode of core solidification in asteroid-sized bodies have meant using the timings and durations of these fields to constrain parent body properties, such as size, is challenging. Here, we use updated equations of state and liquidus relationships for Fe-FeS liquids at low pressures to calculate the locations at which solids form in these cores. We perform these calculations for core-mantle boundary (CMB) pressures from 0 - 2 GPa, and Fe-FeS liquid concentrations on the iron-rich side of the eutectic, as well as two values of iron thermal expansivity that cover the measured uncertainties in this parameter, and adiabatic and conductive cooling of these cores. We predict inward core crystallisation from the CMB in asteroids due to their low < 0.5 GPa pressures regardless of the uncertainties in other key core parameters. However, due to low internal pressures in these cores, remelting of any iron snow, as proposed to generate Ganymede's present day field, may be unlikely as the cores are approximately isothermal. Therefore

*Corresponding author. E-mail: kathryn.dodds@ens-lyon.fr Present address: LGL-TPE, École Normale Supérieure de Lyon, 46 Allée d'Italie, Lyon, 69007, France.

a different mode of inward core solidification is possibly required to explain compositionally-driven dynamo action in asteroids. Additionally, we identify possible regimes at higher $> 0.6 - 2$ GPa pressures in which crystallisation can occur concurrently at the CMB and the centre.

Keywords: Asteroids, Magnetic fields

1. Introduction

The crystallisation of a liquid iron alloy core can be a highly efficient process for generating a self-exciting dynamo (Nimmo (2009), Nimmo (2015)) because it can produce large ($> 1000 \text{ kg m}^{-3}$) density differences and hence buoyancy forces that power convection. For instance, core crystallisation is responsible for the present-day dynamo activity and associated magnetic fields of Earth, Ganymede (Rückriemen et al., 2015) and Mercury (Breuer et al., 2007), as well as potentially for the ancient Moon (Weiss and Tikoo, 2014). Moreover, this process has been proposed to have powered the later periods of dynamo generation in asteroids during the first few hundreds of millions of years after the start of the solar system (Shah et al. (2017), Maurel et al. (2018), Bryson et al. (2019a), Maurel et al. (2020), Nichols et al. (2021)). These rocky worlds span a large range of sizes, from < 100 km radii asteroids, to the Earth whose mean radius is 6734 km, and have experienced accretionary and differentiation histories of varying complexity. These differences have led to varying thermochemical structures within their cores (e.g. Stevenson et al. (1983), Driscoll and Bercovici (2014)), which introduce multiple potential mechanisms for dynamo activity throughout their lifetimes, culminating in the solidification of their cores.

The location at which a planetary body's core starts to solidify depends on where its temperature profile first crosses its liquidus (Figure 1a). For the Earth, the high pressures within the core (> 120 GPa) lead to liquidus temperatures that increase more rapidly with depth than the adiabatic temperature, since it becomes increasingly favourable for iron to exist as a solid rather than a liquid at higher pressures and hence greater depths. Therefore, the Earth's core first cooled below the liquidus at its centre, nucleating an inner core and subsequently generating a dynamo field driven by outwards core crystallisation.

However, the other rocky bodies that are known to have, or previously had, a dynamo are far smaller than the Earth and thus their core pressures

31 are lower, e.g. < 10 GPa for the Moon and Ganymede. This can result in
32 a core liquidus that increases more slowly with depth within the core than
33 the adiabat, causing the first solids to form at the CMB (Figure 1b). Multi-
34 ple dynamo mechanisms have been proposed for inwardly crystallising cores,
35 such as the iron snow model for Ganymede, where iron crystals form at the
36 CMB and sink into the hotter interior. The crystals then remelt, increas-
37 ing the liquid density and driving convection and a dynamo (Rückriemen
38 et al., 2015). Models of dynamo generation during top-down crystallisation
39 in asteroids, e.g. Scheinberg et al. (2016) and Neufeld et al. (2019), have
40 considered delamination of large metre-scale dendrites that stir up the core
41 liquid sufficiently to generate a dynamo as they sink. However, these models
42 have predominantly been developed to explain the magnetization of the IVA
43 iron meteorites and their unmantled parent body, and therefore may not be
44 applicable to typical mantled asteroids.

45 The direction of core solidification is a key factor controlling the mech-
46 anisms by which planets and planetesimals are able to generate dynamos.
47 However, the core crystallisation regime in which the cores of meteorite par-
48 ent bodies lie is uncertain. Both Haack and Scott (1992) and Chabot and
49 Haack (2006) invoke inward core crystallisation to explain the fractional crys-
50 tallisation patterns observed in iron meteorites. The calculations from Haack
51 and Scott (1992), which Chabot and Haack (2006) use to inform their predic-
52 tion of the direction of crystallisation, are limited to pure iron cores because
53 the equations of state and the liquidus behaviour of liquid iron alloys were
54 not available at the time. More recently, Williams (2009) calculated the likely
55 crystallisation regime for small solar system objects such as Ganymede and
56 the Moon for a limited range of core sulfur contents (0, 5, 10 wt% S) based
57 on the relative slopes of the liquidus and adiabat. That study concluded
58 that asteroid cores with pressures < 2 GPa may crystallize either inwardly
59 or outwardly, depending critically on the core’s thermal expansivity, α , and
60 sulfur composition.

61 Since the publication of Williams (2009), updated formulations of both
62 the liquidus behaviour and equations of state of Fe-FeS alloys at low pressure
63 have been published (Buono and Walker (2011), and Rivoldini et al. (2009)
64 and Morard et al. (2018), respectively), which allow for the consideration of
65 a far wider range of core sulfur compositions than was possible by Williams
66 (2009). Additionally, thermal evolution models of asteroids have shown that
67 the CMB heat flux prior to the onset of core solidification may be either sub-
68 or super-adiabatic, depending on core size and sulfur content (Bryson et al.,

69 2019b), whereas Williams (2009) considered only adiabatic heat fluxes. A
70 sub-adiabatic CMB heat flux would lead to a conductive temperature profile
71 within the core with a lower temperature gradient compared to a convecting
72 core, which may then affect its direction of solidification.

73 In this study, we determine the likely direction of core solidification in
74 asteroid-sized bodies over a wider parameter range than was previously pos-
75 sible, using updated liquidus relationships and equations of state for Fe-FeS
76 alloys at low pressures (< 2 GPa). We then use our results to explore which
77 dynamo mechanisms are likely to be applicable to asteroid-sized cores and
78 discuss any outstanding issues in our understanding of compositional dy-
79 namo generation during core solidification for these small rocky bodies. We
80 identify five possible modes of core solidification within this pressure and
81 composition range. For asteroids (i.e., bodies < 600 km in total radius), we
82 predict inward core solidification, regardless of core sulfur composition, in
83 contrast to Williams (2009). For larger bodies, we predict core solidification
84 modes in which crystallisation could occur simultaneously at the centre and
85 the CMB. These modes are relevant to bodies with CMB pressures of > 0.6
86 to > 2 GPa, depending critically on sulfur concentration.

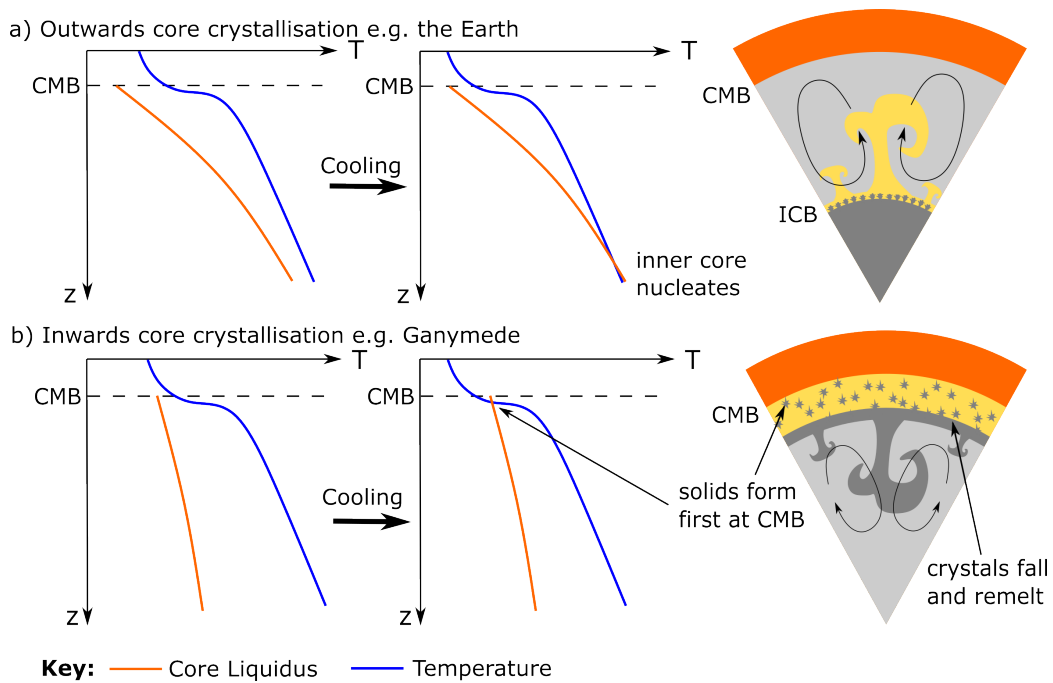


Figure 1: **Schematics of core crystallisation starting from a) the centre of a planet’s core, e.g. the Earth and b) from below its core-mantle boundary e.g. Ganymede.** The location at which the first solids form is governed by where the core’s temperature profile first crosses its liquidus on cooling. This is controlled by the relative slopes of the core liquidus (orange line) and temperature (blue line). The temperature profile in a convecting core lies along an adiabat except within a narrow thermal boundary layer below the CMB (black dashed line). The direction of core crystallisation then controls the mechanism of dynamo generation. In outwardly crystallising cores, e.g. Earth, light-element enriched liquid is expelled from the inner core and rises buoyantly, mixing and driving convection (Loper, 1978). Dynamo generation in top-down crystallising cores is less well understood but Ganymede’s dynamo has been proposed to be driven by the remelting of iron crystals that form at the CMB in its deep interior (Rückriemen et al., 2015).

87 **2. Theory**

88 The location at which a planet’s core starts to solidify depends on the re-
 89 lationship between the thermal structure of the core and that of the liquidus,
 90 or more generally the structure of the phase diagram. Previous studies in-
 91 vestigating the direction of crystallisation in asteroids (e.g. Williams (2009))
 92 used the relative pressure differentials of the core adiabat and liquidus to
 93 determine the expected direction of core solidification. In this linear approx-
 94 imation, outward crystallisation is predicted when

$$\frac{\partial T_c}{\partial P} < \frac{\partial T_l}{\partial P}, \quad (1)$$

95 where $\partial T_c/\partial P$ and $\partial T_l/\partial P$ are the pressure differentials of the core temper-
 96 ature and liquidus, respectively, with pressure acting as a proxy for depth
 97 within the core. Inward crystallisation instead occurs when

$$\frac{\partial T_c}{\partial P} > \frac{\partial T_l}{\partial P}. \quad (2)$$

98 However, this approach may not reveal all the different ways that small
 99 planetary cores can solidify because Bueno and Walker (2011) found that
 100 the liquidus temperature of Fe-FeS liquids first decreases with pressure for
 101 all sulfur contents on the iron-rich side of the eutectic (< 32 wt% S) before it
 102 starts to increase at pressures of 0.75 - 1.50 GPa (Figure 2). This minimum in
 103 the Fe-FeS liquidus at low pressures could lead to simultaneous solidification
 104 at multiple locations within a small planetary core, which in turn would
 105 affect the possible available dynamo driving mechanisms as well as the core’s
 106 thermochemical evolution. Since evaluating only the pressure differentials of
 107 the core temperature and liquidus does not allow us to determine if a core
 108 could crystallise in more than one location contemporaneously, we instead
 109 calculate the temperature and liquidus as a function of pressure within small
 110 planetary cores. In general, the core temperature as a function of pressure
 111 is given by

$$T_c(P) = T_{CMB} + \int_{P_{CMB}}^P \frac{\partial T_c}{\partial P'} dP', \quad (3)$$

112 where T_{CMB} and P_{CMB} are the CMB temperature and pressure respectively,
 113 P' is a dummy variable, and $\partial T/\partial P'$ is the pressure differential of the core

114 temperature, which depends not only on its sulfur concentration and pres-
 115 sure but also on the mechanism of heat transfer in the core at the onset of
 116 solidification, for which both convection and diffusion may have occurred.
 117 To calculate the temperature profile, we use a first-order Taylor expansion
 118 such that

$$T_c(P + \Delta P) = T_c(P) + \left. \frac{\partial T_c(P)}{\partial P} \right|_P \Delta P, \quad (4)$$

119 starting from the CMB, at which we set an initial CMB temperature such
 120 that all depths within the core are initially fully molten.

121 To determine where core crystallisation occurs, we first calculate the liq-
 122 uidus profile within a core of given CMB pressure (Section 2.1). We then
 123 lower the CMB temperature incrementally, recalculating the temperature
 124 profile at each iteration (Section 2.2) to mimic core cooling. For simplicity,
 125 we neglect here both the effect of the release of latent heat during crystallisa-
 126 tion as well as any chemical evolution of the core liquid on the temperature
 127 profile. We anticipate that the inclusion of latent heat and chemical evolu-
 128 tion may alter the time dependence of cooling, but will not significantly alter
 129 the location or mode of early crystallisation. At each temperature step, we
 130 identify any pressures at which the core temperature is below the liquidus
 131 and thus crystallising. We continue lowering the CMB temperature until the
 132 entire core is below the liquidus. This approach allows us to investigate the
 133 potential evolution of core crystallisation as well as its initial location and
 134 direction.

135 In the following sections, we detail the Fe-FeS liquidus surface and equa-
 136 tion of state required to calculate the core temperature and liquidus as a
 137 function of pressure, and so determine the possible regimes in which asteroid
 138 cores crystallise. We vary P_{CMB} between 0 - 2 GPa, which corresponds to
 139 the expected CMB pressures of fully differentiated asteroids that have not
 140 undergone any sufficient mantle stripping during impacts with cores of radii
 141 ≤ 600 km, assuming a core/planetary radius ratio, $R_c/R_p = 0.5$.

142 We also consider both adiabatic and sub-adiabatic CMB heat fluxes, as
 143 previous models of asteroid thermal evolution predict that these cores cooled
 144 conductively for much of their history (Bryson et al., 2019b), including prior
 145 to core solidification. Additionally we consider two values for the thermal
 146 expansivity of liquid iron, $9.2 \times 10^{-5} \text{ K}^{-1}$ and $1.32 \times 10^{-4} \text{ K}^{-1}$ (Williams,
 147 2009), and core sulfur contents of $\leq 32 \text{ wt}\% \text{ S}$ as these two quantities

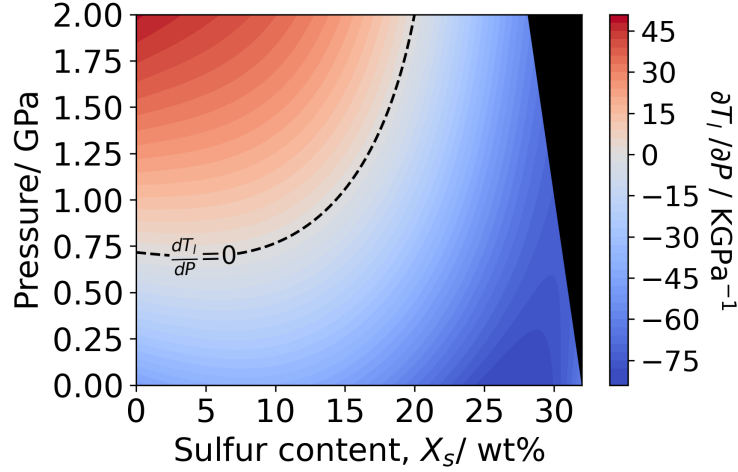


Figure 2: **Pressure derivative of the Fe-FeS Liquidus** as a function of pressure and sulfur content for cores of < 5 GPa (Buono and Walker, 2011). The dashed line separates the high pressure regime (red), where the liquidus temperature increases with pressure, from the low pressure regime (blue) where the liquidus temperature decreases with pressure. The sulfur content of the Fe-FeS eutectic decreases with pressure; the black shaded region at high pressures and high sulfur contents represents super-eutectic Fe-FeS liquids for which the equations of state and liquidus behaviour used here are not valid. In the low pressure regime, regardless of the pressure dependence of the core adiabat, which is always positive, core crystallisation proceeds inwardly from the CMB. In the high pressure regime, both inward and outward core crystallisation are possible. The mode of solidification that operates depends on the pressure dependence of the core adiabat. Finally, for cores with pressures that span the minimum in the liquidus temperature (black dashed line), crystallisation may occur simultaneously at multiple locations.

148 carry large uncertainties due to difficulties associated with measuring them
 149 accurately.

150 *2.1. Pressure dependence of the core liquidus*

151 Based on a compilation of experimental Fe-FeS melting studies, Buono
 152 and Walker (2011) give the pressure and sulfur concentration dependence of
 153 the Fe-FeS liquidus as

$$T_l(X_{mol}^{FeS}, P) = A(P)(X_{mol}^{FeS})^4 + B(P)(X_{mol}^{FeS})^3 + C(P)(X_{mol}^{FeS})^2 + D(P)(X_{mol}^{FeS}) + E(P), \quad (5)$$

154 where X_{mol}^{FeS} is the molar content of FeS in the core, P is the pressure in
 155 GPa and A , B , C , D and E are pressure-dependent constants. The values
 156 of these constants are approximately given by

$$\begin{aligned}
 A(P) &= -2.4724P^4 + 28.025P^3 + 9.1404P^2 + 581.71P + 3394.8, \\
 B(P) &= 1.7978P^4 - 6.7881P^3 - 197.69P^2 - 271.69P - 8219.5, \\
 C(P) &= 0.1702P^4 - 9.3959P^3 + 163.53P^2 - 319.35P + 5698.6, \\
 D(P) &= 0.2308P^4 + 7.1P^3 - 64.118P^2 + 105.98P - 1621.9, \\
 E(P) &= 0.2302P^4 - 5.3688P^3 + 38.124P^2 - 46.681P + 1813.8. \quad (6)
 \end{aligned}$$

157 This formulation for the Fe-FeS liquidus is valid for pressures < 10 GPa,
 158 i.e. for bodies of Ganymede’s size or less, and sulfur contents on the iron-rich
 159 side of the eutectic, with a goodness of fit to their experimental results of
 160 $R^2 = 0.901$ for 1 bar, $R^2 = 0.996$ for 3 GPa (Buono and Walker, 2011).

161 *2.2. Pressure dependence of the core temperature*

162 Models of asteroid thermal evolution, for example by Bryson et al. (2019b),
 163 have shown that asteroid cores likely cooled by conduction prior to core so-
 164 lidification as heat loss out of their silicate mantles at that time was low
 165 (< 10 mW m $^{-2}$). Conductive cooling results in a core temperature profile
 166 that increases less rapidly with depth and pressure compared to convective
 167 cooling, thereby this initial core condition possibly promotes outwards core
 168 solidification.

169 However, these models of asteroid evolution generally consider cores with
 170 a eutectic sulfur concentration which start to crystallise at 1234 K. This
 171 low liquidus temperature leads to core crystallisation occurring late, long
 172 after magma ocean convection ceases, when the body is cooling slowly. From
 173 the iron meteorite record, the inferred sulfur content of asteroid cores is
 174 0 – 14 wt% S (Goldstein et al., 2009). For such low < 14 wt% S cores,
 175 we would expect core crystallisation to begin earlier, i.e. during the period
 176 of magma ocean convection when the CMB heat flux is superadiabatic due
 177 to higher > 1550 K CMB liquidus temperatures (Bryson et al., 2019b)
 178 predicted for low pressure (< 1 GPa) cores. However, many of the lowest
 179 sulfur iron meteorite groups show evidence for impact-driven volatile loss
 180 (Goldstein et al., 2009). Therefore these low inferred sulfur contents may not
 181 represent the original core composition. Nonetheless, it is worth considering

182 low core sulfur concentrations as they could result in cores that convect prior
 183 to the onset of core solidification, and hence possibly favour inwards core
 184 solidification.

185 Given this dependence on sulfur content for the initial core temperature
 186 profile, we therefore calculate the expected regime of core solidification for
 187 both super- and sub-adiabatic CMB heat fluxes to explore the full effect of
 188 CMB heat flux on core crystallisation.

189 *2.2.1. In a convecting core*

190 If a core is convecting, its thermal profile lies along the core adiabat except
 191 in a narrow thermal boundary layer below the CMB (Figure 1). However,
 192 given the low viscosity of the core liquid, both the thickness and tempera-
 193 ture difference across this boundary layer is negligible so we do not include
 194 it in our core temperature profile. In asteroid-sized bodies, this requires
 195 heat fluxes out of the CMB of approximately 10 mW m^{-2} (Bryson et al.,
 196 2019b). Following Williams (2009), the pressure differential of the adiabatic
 197 temperature, T_{ad} , of the core is given by

$$\frac{\partial T_{ad}}{\partial P} = \frac{1}{\rho g(r)} \frac{\partial T_{ad}}{\partial r} = \frac{\alpha}{\rho c_p T_{ad}}, \quad 0 < P < P_{CMB} \quad (7)$$

198 where α , ρ and c_p are the core thermal expansivity, density and specific
 199 heat capacity, respectively. These parameters are all functions of the core
 200 pressure, temperature, and light element concentration. Here we consider
 201 only variations in the sulfur content of these cores, X_s , since sulfur has a
 202 large effect on the core liquidus (Buono and Walker, 2011), as well as density
 203 and thermal parameters such as c_p (Kanda et al., 1986).

204 We take the specific heat capacity to be only a function of sulfur content
 205 over the pressure-temperature range considered here. Following Williams
 206 (2009) and Morard et al. (2018), this is given by linear interpolation between
 207 its value for pure iron, $c_{p,Fe} = 850 \text{ J kg}^{-1} \text{ K}^{-1}$ (Elkins-Tanton et al., 2011),
 208 and its value for pure FeS, $c_{p,FeS} = 454 \text{ J kg}^{-1} \text{ K}^{-1}$ (Kanda et al., 1986).

209 To calculate the density of the Fe-FeS liquid as a function of pressure,
 210 sulfur content and temperature, we follow Morard et al. (2018), who provide
 211 an equation of state for these liquids for $P < 5 \text{ GPa}$, $T < 1900 \text{ K}$, and
 212 $X_s < 32 \text{ wt\% S}$, i.e., the parameter space in which asteroid cores exist.
 213 The pressure dependence of the liquid density is described by a third-order
 214 Birch-Murnaghan equation (Morard et al., 2018), where

$$P = \frac{3}{2}K_{T,0} [f^{7/3} - f^{5/3}] \left[1 + \frac{3}{4} (K'_{T,0} - 4) \right] (f^{2/3}) - 1. \quad (8)$$

215 Here we define

$$f = \frac{\rho_P}{\rho_0}, \quad (9)$$

216 where ρ_P is the density at the required pressure and sulfur content, ρ_0 , is
 217 the reference density of a liquid with the same sulfur content at the reference
 218 pressure of $P = 1$ bar, and both are at a reference temperature of $T_0 = 1900$
 219 K. $K_{T,0}$ is the isothermal bulk modulus of the liquid Fe-FeS evaluated at the
 220 liquidus temperature and $P = 0$ GPa, and $K'_{T,0}$ is the first derivatives of
 221 this modulus with respect to pressure, also evaluated at the same reference
 222 conditions. The reference density as a function of sulfur content is given by

$$\rho_0 = -3108 (X_{mol}^S)^2 - 5176X_{mol}^S + 6950 \quad (10)$$

223 in kg m^{-3} where X_{mol}^S is the core molar sulfur content (Morard et al., 2018).
 224 The isothermal bulk modulus at ambient pressure as a function of molar
 225 sulfur content is given by

$$K_{T,0} = (K_{T,Fe})^{1-X_{mol}^S} \times (K_{T,S})^{X_{mol}^S}, \quad (11)$$

226 where $K_{T,Fe} = 76$ GPa and $K_{T,S} = 1.6$ GPa. While linear mixing
 227 models are often used for bulk moduli, as in Rivoldini et al. (2009), these are
 228 only valid for small compositional ranges. In previous studies, Morard et al.
 229 (2013) and Morard et al. (2018) find this form more suitable for the large
 230 compositional range considered in their experiments. The pressure derivative
 231 of the bulk modulus as a function of molar sulfur content is given by

$$K'_{T,0} = K'_{Fe} + 3X_{mol}^S, \quad (12)$$

232 where $K'_{Fe} = 6.5$ (Morard et al., 2018). Combining Equations 8 and 10
 233 allows us to calculate the liquid density, $\rho(T_0, P, X_S)$, as a function of pressure
 234 and sulfur content at $T_0 = 1900$ K. For the temperature variation of the
 235 density, we assume a linear dependence of density on temperature, following
 236 (Morard et al., 2018) and Williams (2009). This has been shown to be a valid
 237 approximation for Fe liquids by Assael et al. (2006) for $T < 2500$ K. As
 238 such, the density of an Fe-FeS liquid as a function of pressure, temperature
 239 and sulfur content is given by

$$\rho(T, P, X_s) = \rho(T_0, P, X_s) [1 + \alpha(T_0 - T)]. \quad (13)$$

240 Finally, the thermal expansivity of core liquid at a given pressure and
 241 temperature is calculated by

$$\alpha(P, T) = \frac{\alpha_0 K_{T,0}}{K_T(P, T)}, \quad (14)$$

242 where $K_T(P, T)$ is the isothermal bulk modulus of the liquid and $K_{T,0}$ and
 243 α_0 are the isothermal bulk modulus and thermal expansivity at the reference
 244 conditions of $P = 0$ GPa and T , the current core temperature. While this
 245 reference thermal expansivity is technically a function of both temperature
 246 and sulfur concentrations, we assume here that it is constant over the temper-
 247 ature range we are considering as its value has been shown to be constant for
 248 liquid iron at temperatures $T < 2500$ K (Assael et al., 2006). Additionally,
 249 we assume this parameter is constant for all sulfur concentrations as it is not
 250 well constrained for pure liquid iron at low pressures, let alone for intermedi-
 251 ate sulfur concentrations (Williams (2009), Morard et al. (2018)). Therefore
 252 we adopt two values: a high value of $\alpha_0 = 1.3 \times 10^{-4} \text{ K}^{-1}$ (Assael et al.,
 253 2006) and a low value of $\alpha_0 = 9.2 \times 10^{-5} \text{ K}^{-1}$ (Hauck et al., 2006). These
 254 two values cover the range of measured iron and Fe-S thermal expansivities
 255 (Williams, 2009) and reflect the uncertainty in this key parameter.

256 2.2.2. In a conducting core

257 If the CMB heat flux is subadiabatic ($< 10 \text{ mW m}^{-2}$), the core will cool
 258 conductively. Here we consider a sub-adiabatic heat flux of 1 mW m^{-2} to
 259 explore the effect this has on the expected direction of core solidification in
 260 asteroids. In this case, the temperature will increase less rapidly with depth
 261 when compared to the convecting, adiabatic regime. The pressure differential
 262 of this conductive temperature profile is given by

$$\frac{\partial T_c}{\partial P} = -\frac{F_{CMB}}{k_c} \left(\frac{\partial P}{\partial r} \right)^{-1}, \quad (15)$$

263 where F_{CMB} is the CMB heat flux, $k_c = 30 \text{ W m}^{-1} \text{ K}^{-1}$ is the core thermal
 264 conductivity (Opeil SJ et al., 2012) which we assume to be constant over
 265 the pressure range < 2 GPa, and $\partial P/\partial r$ is the pressure gradient in the core,
 266 which is taken to be hydrostatic. Therefore Equation 15 becomes

$$\frac{\partial T_c}{\partial P} = \frac{F_{CMB}}{k_c} \frac{1}{\rho(T, P, X_s)g}, \quad (16)$$

267 where the density of the core liquid is calculated by Equations 8 through 14
 268 and g is the gravitational acceleration at the CMB.

269 3. Results

270 In this section, we present the possible regimes (Figure 3) and regime
 271 maps for the expected direction of core solidification in asteroids (Figure 4)
 272 covering a core pressure range of < 2 GPa and sulfur contents of ≤ 32 wt% S.
 273 We predict five different crystallising regimes for small planetary cores (Fig-
 274 ure 3): Regime I, purely inwards crystallisation; Regime II, initially inwards
 275 crystallisation followed by outwards crystallisation; Regime III, in which
 276 crystallisation starts concurrently at the CMB and at the centre; Regime
 277 IV, initially outwards crystallisation followed by inwards crystallisation; and
 278 Regime V, purely outwards crystallisation.

279 We find that Regime I, in which solidification first occurs at the CMB and
 280 proceeds inwardly for the entirety of core crystallisation (Figure 3a), is the
 281 dominant mode of solidification for both convecting and conducting cores,
 282 especially those with high > 10 wt% S contents and for the high thermal
 283 expansivity value of $\alpha_{Fe} = 13.2 \times 10^{-5} \text{ K}^{-1}$. The maximum permitted
 284 CMB pressure for a low sulfur concentration, < 10 wt% S, convecting core
 285 to undergo purely inwards core crystallisation is 0.6 GPa and 0.7 GPa for
 286 the low and high values of thermal expansivity, respectively (Figure 4a - b).
 287 For higher ~ 20 wt% sulfur concentration, convecting cores, purely inwards
 288 core crystallisation is expected up to CMB pressures > 2.0 GPa for the high
 289 and low values of α_{Fe} , respectively. In a conducting core (Figures 4c - d),
 290 purely inward core crystallisation occurs at pressures up to ~ 0.6 GPa for
 291 low sulfur concentration cores, and pressures of > 2.0 GPa for high sulfur
 292 concentration cores. These lower pressures are permitted as the tempera-
 293 ture gradient within the core is lower for a conducting core compared to a
 294 convecting one. Regardless, for asteroid-like CMB pressures ≤ 0.5 GPa, cor-
 295 responding to a 300 km radius core under a 300 km thick mantle, we predict
 296 that core crystallisation will proceed from the CMB towards the centre for
 297 the entirety of core solidification. This is because the pressure differential of
 298 the Fe-FeS liquidus being negative, that is the liquidus temperature decreases
 299 with depth in these cores (Figure 2), and this result is independent of sulfur

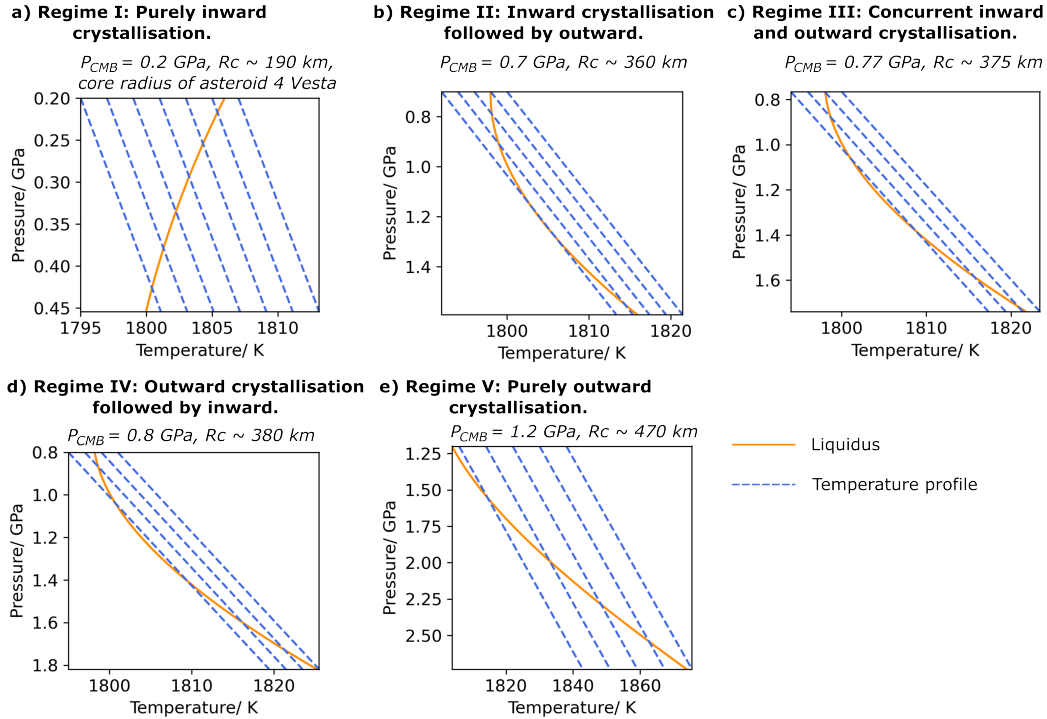


Figure 3: **Examples of the different predicted regimes of core crystallisation** in small planetary cores. For all four examples shown here, the core liquid is pure iron and it is convecting thus the temperature profiles (blue dashed lines) represent the core adiabat, calculated here with $\alpha_{Fe} = 9.2 \times 10^{-5} \text{ K}^{-1}$. We consider the core to be solidifying at pressures where the core adiabat is cooler than the liquidus (solid orange line). Core cooling is approximated by gradually decreasing the CMB temperature, and maintaining a purely adiabatic temperature profile. We find these five regimes are present for all considered sulfur contents and both convecting and conducting cores as their existence is a product of the low pressure liquidus behaviour observed in Fe-FeS liquids. However, the intermediate regimes (II to IV) are restricted to small pressure ranges in conducting cores due to the small temperature gradient in these cores.

300 concentration or the mode of heat transfer within the core at onset time of
 301 core solidification.

302 In Regime II, the core first crystallises at the CMB, and then after con-
 303 tinued cooling, also nucleates an inner core while still freezing in a layer at
 304 the top of the core (Figure 3b). This is possible due to the pressure differen-
 305 tial of the liquidus changing from negative, (i.e. the liquidus decreasing with
 306 depth in the core), to positive, (i.e. the liquidus starts to increase with depth
 307 at intermediate pressures (0.75 - 1.4 GPa, depending on sulfur content)).

308 As a result, after sufficient core cooling, the core temperature profile, which
 309 always increases with depth, can intersect the liquidus profile both at the top
 310 of the core and at the centre. This regime is limited to pressures of 0.6 - 0.8
 311 GPa ($R_c \sim 350 - 370$ km) and 0.8 - 1.0 GPa ($R_c \sim 380 - 420$ km) for a pure
 312 iron, convecting core with the low and high values of α_{Fe} , respectively. For
 313 higher sulfur concentration (> 15 wt% S) and for convecting cores, we do not
 314 observe this regime as the pressure differential of the liquidus is negative in
 315 this region of parameter space. In a conducting core, this regime is confined
 316 to a narrow range of pressures ~ 0.1 GPa higher than the maximum permit-
 317 ted for Regime I for low (< 18 wt% S) sulfur cores. This is due to the small
 318 temperature gradient within these cores, which reduces the likelihood of the
 319 temperature profile crossing the liquidus profile more than once.

320 For very specific combinations of P_{CMB} and X_s , we find that core crys-
 321 tallisation starts concurrently at the CMB and at the centre of these cores
 322 (Regime III, Figure 3c). This is only possible when the overall temperature
 323 difference across the core is equal to the overall difference in liquidus temper-
 324 ature between the CMB and the centre. Therefore, this regime occurs at the
 325 highest pressures for convecting cores with $\alpha_{Fe} = 13.2 \times 10^{-5} \text{ K}^{-1}$ (Figure
 326 4a) and the lowest pressures for conducting cores (Figures 4c - d) as these
 327 cores have the greatest and smallest core temperature gradients, respectively.

328 Cores in regime IV on the other hand are predicted to first nucleate an
 329 inner core and then, after further cooling, start to crystallise at the CMB as
 330 well (Figure 3d). This regime only occurs for pressures greater than those
 331 that define the minimum in the liquidus surface, i.e. pressures over which the
 332 liquidus always increases with depth. At these pressures, the liquidus tem-
 333 perature increases more rapidly with increasing pressure ($\partial^2 T_l / \partial P^2 > 0$).
 334 This results in a concave-up liquidus profile across these cores compared to
 335 the (approximately) linear temperature profile. Therefore, it is possible for
 336 the temperature profile to intersect the liquidus near the top of the core, as
 337 well as at the bottom, and thus for the core to simultaneously crystallise
 338 inwardly from the CMB as well as growing an inner core. Regime IV oc-
 339 curs over a wide parameter range in convecting cores for sulfur contents
 340 < 15 wt% S and pressures from 0.8 GPa up to > 2 GPa ($R_c \sim 380 - >$
 341 600 km) for $\alpha_{Fe} = 9.2 \times 10^{-5} \text{ K}^{-1}$, and for sulfur contents < 13 wt% S
 342 and pressures from 1.0 GPa up to > 2 GPa ($R_c \sim 410 - > 600$ km) for
 343 $\alpha_{Fe} = 13.2 \times 10^{-5} \text{ K}^{-1}$. However in conducting cores, this regime is
 344 restricted to a narrower range of permitted pressures. For a low sulfur, con-
 345 ducting core, it can occur over a small ~ 0.1 GPa pressure range, for example

346 with $X_s = 10$ wt% S, the pressure range is 0.8 - 0.9 GPa ($R_c \sim 380 - 400$
347 km). For higher values of core sulfur content, such as $X_s = 18$ wt% S, regime
348 IV can occur over a wider pressure range from 1.6 - > 2.0 GPa ($R_c \sim 530 -$
349 > 600 km).

350 Finally, it is only possible for low sulfur concentration, high pressure
351 cores to crystallise outwardly throughout their entire solidification (Regime
352 V, Figure 3e). In convecting cores, sulfur contents < 13 wt% S and pressures
353 > 1.2 GPa ($R_c > 500$ km) are required for $\alpha_{Fe} = 9.2 \times 10^{-5} \text{ K}^{-1}$, in
354 order for core crystallisation to be completely outward. For the higher value
355 of $\alpha_{Fe} = 13.2 \times 10^{-5} \text{ K}^{-1}$, sulfur contents < 8 wt% S and pressures
356 > 1.5 GPa ($R_c > 510$ km) are instead required. If the core is conducting at
357 the start of core crystallisation, purely outwards core solidification is possible
358 at lower pressures due to the smaller temperature gradient within these cores.
359 For a low sulfur core, this could occur in cores with $P_{CMB} > 0.8$ GPa, for
360 example in a core radius of 360 km, whereas in high sulfur cores, this requires
361 pressures > 1.5 GPa, corresponding to cores with radii > 510 km.

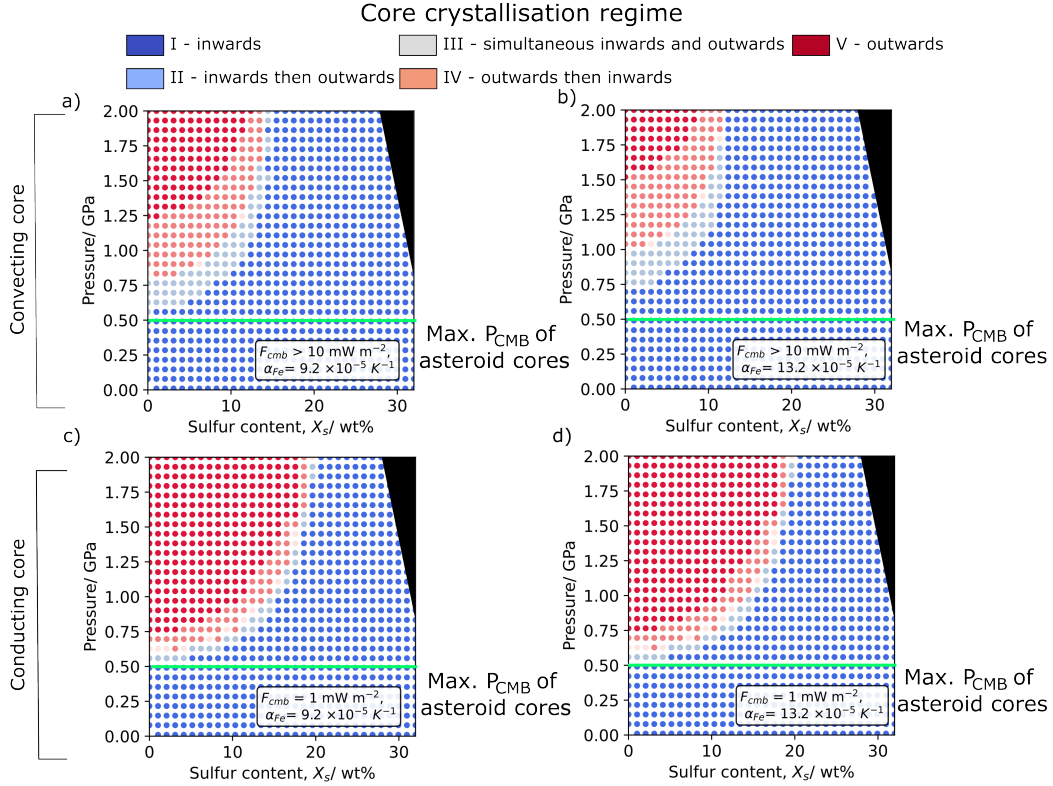


Figure 4: **Expected directions of core solidification as a function of CMB pressure, core sulfur content, CMB heat flux and the thermal expansivity of liquid iron.** The regimes are defined in Figure 3. The black shaded region indicates super-eutectic Fe-FeS liquids for which the liquidus surface given in Buono and Walker (2011) is no longer valid. The maximum expected P_{CMB} for asteroids is ~ 0.5 GPa, which could correspond to an asteroid with a core radius of ~ 300 km and total radius of ~ 600 km.

362 4. Discussion

363 4.1. Comparison to previous studies

364 Our results show that inward core solidification is the dominant direction
365 in cores with CMB pressures < 0.5 GPa, regardless of sulfur concentration or
366 mode of heat transfer. By contrast, outwards core solidification is restricted
367 to large, low sulfur cores. For a convecting core, the minimum pressure re-
368 quired for core solidification to begin at the centre is 1.2 GPa and 1.5 GPa for
369 high and low thermal expansivities, respectively, and these minimum pres-
370 sures require a pure iron core. Higher core sulfur contents raise the minimum
371 pressure requirement further (Figure 4) while lower sub-adiabatic heat fluxes
372 allow for smaller, more sulfur-rich cores (Figure 4 c-d) initially to crystallise
373 outwardly. However, even in the most favourable conditions (Regime V), the
374 minimum pressure required for purely outwards crystallisation corresponds
375 to a 360 km core radius, (i.e., > 720 km radius body). This would make
376 such a body significantly larger than Ceres, the largest object in the asteroid
377 belt at present day with a radius of 473 km. Therefore we consider inward
378 solidification to be the most likely direction of core crystallisation in the vast
379 majority of asteroids, regardless of sulfur content or core thermal expansivity.
380 This is in agreement with Haack and Scott (1992) and Chabot and Haack
381 (2006), both of which predict inward core crystallisation for pure iron cores.

382 However, our results differ from those of Williams (2009) in which out-
383 wards core solidification is predicted for pure iron cores at all pressures when
384 the lower bound of thermal expansivity $\alpha_{Fe} = 9.2 \times 10^{-5} \text{ K}^{-1}$ is used. This
385 difference stems from the descriptions of the pressure differential of the liq-
386 uidus $\partial T_l / \partial P$ in the two studies. Williams (2009) adopts a constant value of
387 $\partial T_l / \partial P \approx 35 \text{ K GPa}^{-1}$ from Strong et al. (1973), whereas we have adopted
388 an updated liquidus relationship from Buono and Walker (2011) that cov-
389 ers a larger pressure and composition range than Strong et al. (1973). This
390 updated liquidus relationship results in a liquidus slope that varies consid-
391 erably with both these variables (Figure 2). This includes a low pressure
392 region ($P < 0.7$ GPa) where $\partial T_l / \partial P < 0$ and thus inward solidification is
393 expected for all sulfur contents. However, the behaviour of Fe-FeS liquidus
394 is not well studied experimentally at pressures < 2 GPa, with more atten-
395 tion being targeted at the intermediate 5 – 10 GPa and high $P \gg 10$ GPa
396 pressures relevant to both Ganymede and the Moon, and the Earth’s core,
397 respectively (Morard et al. (2007) and Morard et al. (2014)). Therefore, the
398 true behaviour of the Fe-FeS liquidus for pressures relevant to asteroid-sized

399 bodies is a key outstanding uncertainty in these thermodynamic calculations,
400 and further refinement would allow for more accurate determination of the
401 expected core crystallisation direction.

402 Williams (2009) also considers the effect of core sulfur content on the
403 direction of core solidification. However, this previous study only considered
404 values of 5 wt% S and 10 wt% S whereas we consider all compositions on
405 the iron-rich side of the Fe-FeS eutectic. Inward crystallisation is predicted
406 for 10 wt% S cores for $P < 10$ GPa regardless of the choice of α_{Fe} , and for
407 5 wt% S cores for $P < 10$ GPa and $P < 4.5$ GPa with $\alpha_{\text{Fe}} = 13.2 \times 10^{-5} \text{ K}^{-1}$
408 and $\alpha_{\text{Fe}} = 9.2 \times 10^{-5} \text{ K}^{-1}$, respectively. Our study predicts that inward
409 solidification will only occur at significantly lower pressures ($< 0.8 - 1.2$ GPa)
410 than these for same sulfur concentrations (Figures 4a - b). This difference
411 is again due to the different liquidus maps used in each study. However, the
412 pressures at which we predict outwards core solidification in convecting low
413 S cores are still greater than those expected in asteroid-size cores. Therefore
414 we still expect inwards to be the dominant solidification direction in asteroid
415 cores. Additionally, our results indicate that for a given pressure and core
416 size, the addition of sulfur promotes inward core solidification, in agreement
417 with the conclusion of Williams (2009).

418 We have also identified three other possible regimes of core solidification in
419 which crystallisation can occur concurrently in multiple locations throughout
420 the core (Figures 3b - d). These three regimes are possible in small planetary
421 cores due to the positive second pressure differential of the liquidus in this
422 region of parameter space, which can result in two intersections of the liquidus
423 and core temperature profiles. While it has not been predicted previously,
424 we are able to identify those regimes because we calculate the temperature
425 and liquidus profiles across the cores, instead of relying on the relative slopes
426 of these quantities.

427 The dynamical effect of multiple freezing locations on the evolution of a
428 planetary core is not well explored. Crystallising at both the CMB and at the
429 centre will affect the distribution of latent heat production and light element
430 release on solidification within the core, possibly providing multiple sources
431 of buoyancy fluxes that could drive convection and a dynamo field. Breuer
432 et al. (2015) find that for a super-eutectic Fe-FeS core, crystallisation of FeS
433 solids could first occur in a layer between the CMB and the centre, with the
434 less dense FeS solids then floating upwards towards the CMB and the Fe-
435 enriched fluids sinking downwards. They consider that dynamo generation
436 in this case could be driven by convection caused by the sinking Fe-enriched

437 fluids into the more S-enriched interior, while the solid FeS crystals float
 438 passively upwards and do not contribute to the large-scale convective flow
 439 within the core (Rückriemen et al., 2015). However, in the regimes we have
 440 identified here, crystallisation at the CMB and at the centre could both
 441 produce density differences between two fluid phases, which in turn could
 442 generate convection and a dynamo. There is therefore a need to quantify
 443 the effect of core solidification in multiple locations on the convective power
 444 generated during this process.

445 Additionally, including the full thermochemical evolution of these small
 446 planetary cores during solidification could promote simultaneous crystalli-
 447 sation at the CMB and centre. In this study, our method for simulating
 448 core cooling and solidification only involves decreasing the core temperature.
 449 We have neglected any possible chemical changes in the core fluid during
 450 fractional crystallisation, and hence we have neglected the effect of a slowly
 451 evolving bulk concentration on the core liquidus. For example, for a core that
 452 initially nucleates in the centre but for which the liquidus pressure differen-
 453 tial ($\partial T_l/\partial P > 0$) is close to the turning point, e.g. Regime IV (Figure 3d),
 454 expulsion of sulfur from the growing solid inner core will increase the sulfur
 455 content of the liquid outer core. This in turn will decrease $\partial T_l/\partial P$, which will
 456 eventually become negative and lead to the onset of inward crystallisation as
 457 the inner core continues to grow. Similarly, Regime II in which inwards crys-
 458 tallisation starts first before an inner core is also formed could occur across
 459 a wider parameter range than suggested here. Such an evolution of the bulk
 460 liquid concentration would require any solid iron that formed at the CMB
 461 to fall into the core’s interior and remelt, enriching the interior core fluid in
 462 iron. This would then increase $\partial T_l/\partial P$ of the liquid inner core and could lead
 463 to inner core nucleation. Therefore, including the chemical evolution of the
 464 core during crystallisation would likely act to drive these cores rapidly into a
 465 state with concurrent inward and outward crystallisation, assuming efficient
 466 segregation of the solid and liquid fractions. However, we would not predict
 467 this behaviour for asteroid-sized bodies with $P_{CMB} < 0.5$ GPa as they lie
 468 firmly in Regime I regardless of sulfur content, and are therefore predicted to
 469 solidify inwardly, regardless of any chemical changes within the core liquid.

470 Finally, the intermediate pressures from 0.6 GPa to > 2 GPa over which
 471 Regimes II-IV operate are unlikely to be relevant for asteroid cores, in which
 472 $P_{CMB} < 0.5$ GPa. These regimes may be relevant for the cores of larger
 473 planetary bodies such as the Moon ($P_{CMB} \sim 4 - 5$ GPa), Ganymede
 474 ($P_{CMB} \sim 5 - 7$ GPa), and Mercury ($P_{CMB} \sim 3$ GPa), especially for

475 high core sulfur concentrations. It would therefore be interesting to extend
476 the pressure range considered here up to these higher pressures for which
477 both the equation of state from Morard et al. (2018) and the liquidus surface
478 from Buono and Walker (2011) are valid, and in particular to investigate the
479 possibility of whether these cores could crystallise simultaneously in more
480 than one location.

481 *4.2. Implications for dynamo activity in asteroid cores*

482 Compositionally driven dynamo activity during inward core solidification
483 must be driven by the sinking of the dense pure iron phase formed below the
484 CMB, in contrast to the geodynamo which is driven by buoyant light-element
485 enriched liquid expelled at the inner core boundary. The mechanism of dy-
486 namo generation during inward core solidification has been studied mainly
487 in the context of Jupiter’s largest moon, Ganymede, which has an active dy-
488 namo field at the present day (Kivelson et al. (1996), Gurnett et al. (1996),
489 Sarson et al. (1997)). The current favoured mechanism is the iron snow
490 model, in which iron crystals form below the CMB, sink into the interior
491 where the adiabat is hotter than the liquidus, and they remelt. This remelt-
492 ing produces a pure iron liquid at shallow depths within Ganymede’s core that
493 is denser than the bulk iron-sulfur liquid of the interior. The sinking of this
494 dense iron-rich liquid then produces turbulent convection. This rain-driven
495 convection has been shown by both numerical (e.g., Christensen (2015)) and
496 experimental (e.g., Olson et al. (2017)) methods to produce sufficient entropy
497 to drive Ganymede’s observed dynamo field.

498 However, the small size of asteroid cores (radii of < 300 km) compared
499 to that of Ganymede (radius of ~ 820 km (Rückriemen et al., 2015)) may
500 prevent remelting of any iron snow that forms due to the negligible increase
501 (5 - 10 K) in the adiabatic temperature between their CMBs and core centres.
502 For this reason, previous studies of asteroid core thermal evolution such as
503 Haack and Scott (1992), Scheinberg et al. (2016) and Neufeld et al. (2019)
504 have assumed that their cores are effectively isothermal.

505 Furthermore, recent studies such as Huguet et al. (2018) and Davies et al.
506 (2019) suggest that significant undercooling of > 100 K may be required be-
507 fore iron liquid starts to crystallise, even at the low pressures of asteroid
508 cores. This undercooling would further hinder the remelting of iron crystals
509 as the deep interior of the asteroids’ cores would necessarily be colder than
510 the liquidus at all depths due to this undercooling. Lower degrees of super-
511 cooling could be possible if heterogenous nucleation sites are available, but

512 this possibility has not been studied for any sized planetary core.

513 If the remelting of these iron crystals does not occur, the buoyancy flux
514 required for an iron snow dynamo does not exist in an asteroid core. As
515 such, another mechanism is required. In the iron snow model, the solid iron
516 crystals themselves are assumed to fall passively through the snow zone at
517 the top of the core and not contribute to powering the dynamo due to their
518 assumed sub-millimetre-scale size (Rückriemen et al., 2015). However it is
519 possible that this assumption is not correct. For example, the settling of
520 sediment particles from buoyant plumes into the water column below the
521 plumes has been shown experimentally to drive convection in settings such
522 as estuaries and coastal currents (Hoyal et al., 1999). Additionally, a recent
523 experimental study of the iron snow model has shown that this mode of
524 crystallisation can produce a crystal population with a wide range of sizes
525 (Huguet et al., 2023), which could then interact with the core fluid in a
526 range of different ways from falling passively to stirring up additional flow.
527 Therefore, analogue experiments that mimic inward core crystallisation, such
528 as Huguet et al. (2023), may be key to unravelling the physics that the current
529 iron snow models may be missing.

530 Previous studies of dynamo generation in asteroids have generally fo-
531 cussed on the mechanisms by which unmantled bodies can generate a field,
532 such as Scheinberg et al. (2016) and Neufeld et al. (2019), as they have sought
533 to explain the magnetisation of the rapidly cooled IVA iron meteorites. For
534 example, Neufeld et al. (2019) argues for the periodic delamination of the
535 base of an iron crust at the surface of the IVA parent body, and subsequent
536 dynamo generation driven by stirring of the core fluid as this delaminated
537 layer falls to the centre of the core. These delamination episodes occur suf-
538 ficiently frequently (every ~ 30 kyr) in an unmantled asteroid to generate
539 a continuous Myr-long dynamo. However, given the orders of magnitude
540 slower core cooling rates of the cores of mantled asteroids compared to un-
541 mantled ones, the timescales of delamination in a mantled core are likely to
542 be significantly slower and thus the falling crystals may not stir up the core
543 liquid regularly enough to sustain a continuous field.

544 To summarise, there are difficulties in applying existing models of dynamo
545 generation in inwardly crystallising planetary cores to the cores of most mete-
546 orite parent bodies, and thus to interpret the meteorite paleomagnetic record
547 of asteroid core solidification. This is due to their small size in the case of the
548 iron snow model and slow cooling rates in the case of the dendritic delami-
549 nation models. Therefore, we may require adjustments to these pre-existing

550 models, or an entirely new mechanism for dynamo generation, to explain the
551 late period of magnetic field generation during core crystallisation in mete-
552 orite parent bodies from 65 – 250 Myr (Shah et al. (2017), Morard et al.
553 (2018), Bryson et al. (2019a), Maurel et al. (2020), Nichols et al. (2021)).
554 Such further work would then enable us to build accurate models of this
555 process for use in constraining the sizes of these extinct planetary bodies.

556 5. Conclusions

- 557 • We predict that the cores of most asteroids crystallise inwardly, re-
558 gardless of their light element concentration or any uncertainties in
559 the exact value of the core thermal expansivity. This is based on an
560 improved understanding of both the Fe-FeS liquidus surface and the
561 equation of state at low pressures.
- 562 • We also show that it may be possible for the cores of larger bodies
563 ($R_c \sim 360 - > 600$ km, depending on sulfur content) to solidify simul-
564 taneously at the CMB and centres. This is due to the low pressure
565 turning point of the Fe-FeS liquidus temperature. However, the rele-
566 vance of such regimes to any body in our own Solar System is unclear.
567 Further work is required to explore the effect of multiple freezing points
568 on the thermochemical evolution of the core, and subsequent dynamo
569 potential, as well as extending this study to include higher pressures
570 relevant to the Moon, Mercury and Ganymede to test whether any of
571 these bodies could lie in these regimes.
- 572 • Dynamo generation during asteroid core solidification must therefore
573 be driven by density differences generated at the core-mantle boundary.
574 However, the iron snow model of dynamo generation is unlikely to ap-
575 ply to asteroid-sized cores due to their minimal adiabatic temperature
576 differences, which prevent the remelting of pure iron crystals as they
577 sink. Instead, a new dynamo mechanism is likely required to explain
578 the period of dynamo generation during asteroid core crystallisation as
579 observed in the meteorite paleomagnetic record across several parent
580 asteroids.

581 6. Acknowledgements

582 This work was funded by NERC grant number NE/L002507/1.

583 **7. Data availability**

584 The numerical data produced in this work can be found in ?.

585 **References**

- 586 Assael, M.J., Kakosimos, K., Banish, R.M., Brillo, J., Egry, I., Brooks, R.,
587 Quedstedt, P.N., Mills, K.C., Nagashima, A., Sato, Y., et al., 2006. Refer-
588 ence data for the density and viscosity of liquid aluminum and liquid iron.
589 *Journal of physical and chemical reference data* 35, 285–300.
- 590 Breuer, D., Hauck, S.A., Buske, M., Pauer, M., Spohn, T., 2007. Interior
591 evolution of Mercury. *Space Science Reviews* 132, 229–260.
- 592 Breuer, D., Rueckriemen, T., Spohn, T., 2015. Iron snow, crystal floats,
593 and inner-core growth: modes of core solidification and implications for
594 dynamos in terrestrial planets and moons. *Progress in Earth and Planetary*
595 *Science* 2, 39.
- 596 Bryson, J.F.J., Neufeld, J.A., Nimmo, F., 2019b. Constraints on asteroid
597 magnetic field evolution and the radii of meteorite parent bodies from
598 thermal modelling. *Earth and Planetary Science Letters* 521, 68–78.
- 599 Bryson, J.F.J., Weiss, B., Getzin, B., Abrahams, J., Nimmo, F., Scholl,
600 A., 2019a. Paleomagnetic evidence for a partially differentiated ordinary
601 chondrite parent asteroid. *Journal of Geophysical Research: Planets* 124,
602 1880–1898.
- 603 Buono, A.S., Walker, D., 2011. The Fe-rich liquidus in the Fe-FeS system
604 from 1 bar to 10 GPa. *Geochimica et Cosmochimica Acta* 75, 2072–2087.
- 605 Chabot, N., Haack, H., 2006. Evolution of asteroidal cores. *IIC* 7, 1–0.
- 606 Christensen, U.R., 2015. Iron snow dynamo models for Ganymede. *Icarus*
607 247, 248–259.
- 608 Davies, C.J., Pozzo, M., Alfè, D., 2019. Assessing the inner core nucleation
609 paradox with atomic-scale simulations. *Earth and Planetary Science Let-*
610 *ters* 507, 1–9.

- 611 Driscoll, P., Bercovici, D., 2014. On the thermal and magnetic histories of
612 Earth and Venus: Influences of melting, radioactivity, and conductivity.
613 *Physics of the Earth and Planetary Interiors* 236, 36–51.
- 614 Elkins-Tanton, L.T., Weiss, B.P., Zuber, M.T., 2011. Chondrites as samples
615 of differentiated planetesimals. *Earth and Planetary Science Letters* 305,
616 1–10.
- 617 Goldstein, J., Scott, E., Chabot, N., 2009. Iron meteorites: crystallization,
618 thermal history, parent bodies, and origin. *Chemie der Erde-Geochemistry*
619 69, 293–325.
- 620 Gurnett, D., Kurth, W., Roux, A., Bolton, S., Kennel, C., 1996. Evidence
621 for a magnetosphere at Ganymede from plasma-wave observations by the
622 Galileo spacecraft. *Nature* 384, 535–537.
- 623 Haack, H., Scott, E.R., 1992. Asteroid core crystallization by inward den-
624 dritic growth. *Journal of Geophysical Research: Planets* 97, 14727–14734.
- 625 Hauck, S.A., Aurnou, J.M., Dombard, A.J., 2006. Sulfur’s impact on core
626 evolution and magnetic field generation on Ganymede. *Journal of Geo-
627 physical Research: Planets* 111.
- 628 Hoyal, D.C., Bursik, M.I., Atkinson, J.F., 1999. Settling-driven convection:
629 A mechanism of sedimentation from stratified fluids. *Journal of Geophys-
630 ical Research: Oceans* 104, 7953–7966.
- 631 Huguet, L., Le Bars, M., Deguen, R., 2023. A laboratory model for iron snow
632 in planetary cores. *Geophysical Research Letters* 50, e2023GL105697.
- 633 Huguet, L., Van Orman, J.A., Hauck II, S.A., Willard, M.A., 2018. Earth’s
634 inner core nucleation paradox. *Earth and Planetary Science Letters* 487,
635 9–20.
- 636 Kanda, M., Hasegawa, N., Itagaki, K., Yazawa, A., 1986. Thermodynamic
637 study of the liquid Fe-S system by use of a drop calorimeter. *Thermochim-
638 ica acta* 109, 275–284.
- 639 Kivelson, M., Khurana, K., Russell, C., Walker, R., Warnecke, J., Cor-
640 niti, F., Polanskey, C., Southwood, D., Schubert, G., 1996. Discovery of
641 Ganymede’s magnetic field by the Galileo spacecraft. *Nature* 384, 537–541.

- 642 Loper, D.E., 1978. The gravitationally powered dynamo. *Geophysical Journal International* 54, 389–404.
643
- 644 Maurel, C., Bryson, J.F., Lyons, R.J., Ball, M.R., Chopdekar, R.V., Scholl,
645 A., Ciesla, F.J., Bottke, W.F., Weiss, B.P., 2020. Meteorite evidence for
646 partial differentiation and protracted accretion of planetesimals. *Science*
647 *Advances* 6, eaba1303.
- 648 Maurel, C., Bryson, J.F.J., Weiss, B.P., Scholl, A., 2018. Paleomagnetic
649 evidence for a layered partially differentiated iron-meteorite parent body.
650 *Lunar and Planetary Science Conference* .
- 651 Morard, G., Andrault, D., Antonangeli, D., Bouchet, J., 2014. Properties of
652 iron alloys under the Earth’s core conditions. *Comptes Rendus Geoscience*
653 346, 130–139.
- 654 Morard, G., Bouchet, J., Rivoldini, A., Antonangeli, D., Roberge, M.,
655 Boulard, E., Denoeud, A., Mezouar, M., 2018. Liquid properties in the Fe-
656 FeS system under moderate pressure: tool box to model small planetary
657 cores. *American Mineralogist: Journal of Earth and Planetary Materials*
658 103, 1770–1779.
- 659 Morard, G., Sanloup, C., Fiquet, G., Mezouar, M., Rey, N., Poloni, R., Beck,
660 P., 2007. Structure of eutectic Fe-FeS melts to pressures up to 17 GPa:
661 implications for planetary cores. *Earth and Planetary Science Letters* 263,
662 128–139.
- 663 Morard, G., Siebert, J., Andrault, D., Guignot, N., Garbarino, G., Guyot,
664 F., Antonangeli, D., 2013. The earth’s core composition from high pressure
665 density measurements of liquid iron alloys. *Earth and Planetary Science*
666 *Letters* 373, 169–178.
- 667 Neufeld, J.A., Bryson, J.F.J., Nimmo, F., 2019. The top-down solidifica-
668 tion of iron asteroids driving dynamo evolution. *Journal of Geophysical*
669 *Research: Planets* .
- 670 Nichols, C.I., Bryson, J.F., Cottrell, R.D., Fu, R.R., Harrison, R.J., Herrero-
671 Albillos, J., Kronast, F., Tarduno, J.A., Weiss, B.P., 2021. A time-resolved
672 paleomagnetic record of main group pallasites: Evidence for a large-cored,
673 thin-mantled parent body. *Journal of Geophysical Research: Planets* 126,
674 e2021JE006900.

- 675 Nimmo, F., 2009. Energetics of asteroid dynamos and the role of composi-
676 tional convection. *Geophysical Research Letters* 36.
- 677 Nimmo, F., 2015. Energetics of the core. *Treatise on geophysics* 8, 27–55.
- 678 Olson, P., Landeau, M., Hirsh, B.H., 2017. Laboratory experiments on rain-
679 driven convection: Implications for planetary dynamos. *Earth and Plane-
680 tary Science Letters* 457, 403–411.
- 681 Opeil SJ, C., Consolmagno SJ, G., Safarik, D., Britt, D., 2012. Stony me-
682 teorite thermal properties and their relationship with meteorite chemical
683 and physical states. *Meteoritics & Planetary Science* 47, 319–329.
- 684 Rivoldini, A., Van Hoolst, T., Verhoeven, O., 2009. The interior structure of
685 Mercury and its core sulfur content. *Icarus* 201, 12–30.
- 686 Rückriemen, T., Breuer, D., Spohn, T., 2015. The Fe snow regime in
687 Ganymede’s core: A deep-seated dynamo below a stable snow zone. *Jour-
688 nal of Geophysical Research: Planets* 120, 1095–1118.
- 689 Sarson, G., Jones, C., Zhang, K., Schubert, G., 1997. Magnetoconvection
690 dynamos and the magnetic fields of Io and Ganymede. *Science* 276, 1106–
691 1108.
- 692 Scheinberg, A., Elkins-Tanton, L., Schubert, G., Bercovici, D., 2016. Core so-
693 lidification and dynamo evolution in a mantle-stripped planetesimal. *Jour-
694 nal of Geophysical Research: Planets* 121, 2–20.
- 695 Shah, J., Bates, H.C., Muxworthy, A.R., Hezel, D.C., Russell, S.S., Genge,
696 M.J., 2017. Long-lived magnetism on chondrite parent bodies. *Earth and
697 Planetary Science Letters* 475, 106–118.
- 698 Stevenson, D.J., Spohn, T., Schubert, G., 1983. Magnetism and thermal
699 evolution of the terrestrial planets. *Icarus* 54, 466–489.
- 700 Strong, H., Tuft, R., Hanneman, R., 1973. The iron fusion curve and γ - δ -l
701 triple point. *Metallurgical Transactions* 4, 2657–2661.
- 702 Weiss, B.P., Tikoo, S.M., 2014. The lunar dynamo. *Science* 346, 1246753.
- 703 Williams, Q., 2009. Bottom-up versus top-down solidification of the cores of
704 small solar system bodies: Constraints on paradoxical cores. *Earth and
705 Planetary Science Letters* 284, 564–569.